

Chapter 2

Modelling of Flexible Structures

In this chapter, the design and implementation of the experimental plant and the models used to simulate the experimental plant are discussed. The purpose for the modeling is outlined and the reasons for choosing the experimental plant, and the modeling steps, are given. The description of the cantilever beam used in the experimental plant is followed by a description of the analytical method used to obtain the mathematical models of the plant. The implementation of the simulation models is then discussed.

2.1 Introduction

As mentioned in Chapter 1, an experimental plant together with its mathematical representation are required as a design and evaluation tool for the proposed controllers.

Once the experimental plant is selected, modeling methods can then be applied to find models that represent the experimental plant. Using these models the dynamics of the plant can be studied. As all of the proposed control methods employ natural frequency as the controller parameter, the modeling methods are focused on finding models with accurate representations of the natural frequencies of the systems studied.

The mathematical model of a flexible structure is derived using fundamental theories of physics and mathematics such as Newton's laws, Hooke's laws, Lagrange's equations, Hamilton's principle, etc. The mathematical model that is obtained is known as the equation of motion, which is usually given in the form of a Partial Differential Equation (PDE). To determine the dynamics of the model, the solution of the PDE needs to be found. There are two common methods used to find the solution of the PDE: the analytical method and the numerical method.

The analytical method gives an exact solution of the PDE. The solution is in a closed form and is expressed in terms of known functions. Although analytical methods can be used to very accurately describe the dynamics of structures, the types of applications where this method can be applied are limited. The analytical method is only applicable for systems that are characterized by uniformly distributed parameters and simple boundaries [92]. In many cases, even though closed-form solutions may be possible, great effort and time are required to obtain them. Therefore in practice the analytical method has fewer application areas than the numerical method.

In the numerical method, a discrete version of the model is produced. The spatial dependence in the solution of the PDE is eliminated by applying spatial discretization and the differential eigenvalue problems are transformed into an algebraic form [91]. Several methods exist for constructing the discrete model [27, 91, 92]: Rayleigh's method, Rayleigh-Ritz's method, Galerkin's method, assumed-modes method, collocation method, Holzer's method, Myklestad's method and the finite element method (FEM). FEM is currently the most widely used method for representing discrete models [92]. The FEM package ANSYSTM is used here to study the dynamics of the structures. Due to the use of approximation, numerical methods do not give the same exact results as analytical methods. However,

improvements in the computational power of computers and improvements to approximation algorithms have led to accuracy improvements for the numerical method.

Computer simulation is an important step in the control design process. It provides a flexible and relatively inexpensive means by which to study the dynamics of a plant, design controllers, and evaluate the performances of the controllers prior to their implementation in an actual system. The computer based simulation tool SimulinkTM is used for the simulations. To use Simulink simulation models derived from the modification of the mathematical models obtained from the analytical method or from the modification of the numerical models obtained from the numerical method, need to be implemented.

The implementation of the models is undertaken in four steps. In the first step, the experimental plant (experimental models), which consists of the cantilevered beam and associated loads is built. In the second step, analytical models of the experimental models are derived. In the third step, numerical models of the experimental models are built using ANSYS. The numerical models are then compared with the analytical models and the experimental models to determine their accuracy. In the fourth step, the numerical models are used to construct the simulation models in Simulink.

2.2 Description of Experimental Plant (Experimental Model)

A cantilever beam carrying relatively heavy loads mounted along the beam can serve as a basic representative model for a number of flexible structures such as robot arms and aircraft wings [137, 138]. If the loading on the structure is changed the natural frequencies of the system will change. Depending on the locations and mass of the loads, relatively drastic changes in the natural frequencies can

be experienced.

For a cantilever beam, the sensitivity of a sensor to different modes of vibration, and the authority of an actuator in attenuating the different modes of vibration are determined by the position of the sensor-actuator pair along the beam. For an actuator to have maximum authority over a specific mode it must be placed at the position where the curvature is maximum for that particular mode [27]. The same also applies for the sensitivity of the sensor. Because there is a high average strain at the root of a cantilever structure, maximum sensitivity and control authority can be achieved by placing the sensor-actuator pair close to the root of the structure [42, 63, 153].

The schematic of the experimental plant is shown in Fig. 2.1. A uniform mild steel beam with two identical bonded piezoceramic patches, and two magnetically clamped loads, M_1 and M_2 are mounted in a cantilever arrangement to a concrete block. The piezoceramics are 50mm×50mm PSI-5A4E, 1.02 mm thick patches, placed 1 cm from the root of the beam in order to obtain the maximum sensitivity and control authority. The top patch is used as an actuator and the bottom patch is used as a sensor. The properties of the beam are shown in Table 2.1.

Property	Notation	Value
Length	L	500 (mm)
Width	w	50 (mm)
Thickness	h	3 (mm)
Mass	m	589.5 (gram)
Cross section area	A	150 (mm ²)
Mass density	ρ	7860 (kg/m ³)
Elastic modulus	E	210 (GPa)

Table 2.1. Properties of the beam.

From this configuration, four different experimental models with different loading conditions are tested. The models referred to as Model 1, Model 2, Model 3 and Model 4 are illustrated in Figs. 2.2(a), (b), (c) and (d), respectively.

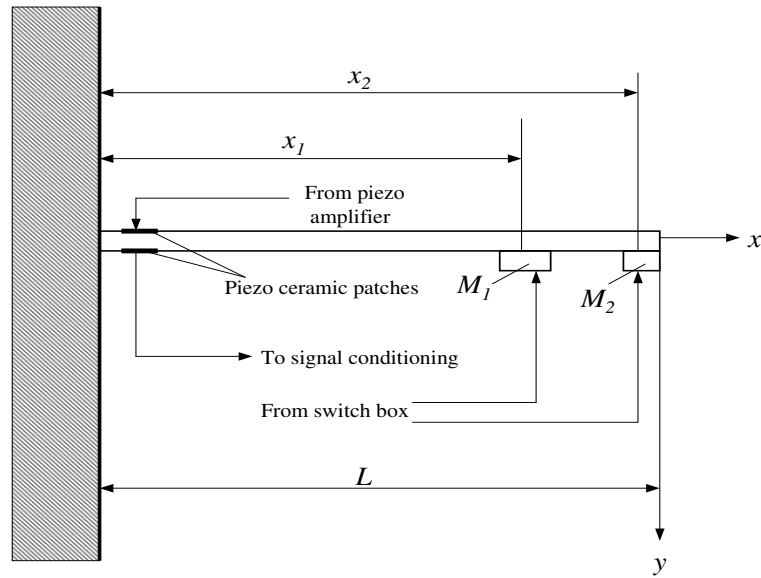


Figure 2.1. Plant with a collocated sensor-actuator pair.

The parameters of the models are shown in Table 2.2. In Model 1, two masses M_1 and M_2 are attached at x_1 and x_2 , respectively. In Model 2 only M_2 is attached to the beam. In Model 3 only M_1 is attached to the beam. Model 4 is a cantilever beam with no attached masses. The positions of x_1 and x_2 are chosen arbitrarily within the broad consideration that the closer the attached masses are to the free end of the beam the lower the natural frequencies of the structures.

Parameter	Notation	Value
Position of load 1	x_1	350 (mm)
Mass of load 1	M_1	283.3 (gram)
Position of load 2	x_2	475 (mm)
Mass of load 2	M_2	193.4 (gram)

Table 2.2. Model parameters.

The natural frequencies of the experimental models are the most important parameters to be considered for the proposed control methods. Therefore, a series of experiments are undertaken to measure the natural frequencies of the four experimental models. The natural frequencies are obtained by applying a sweep

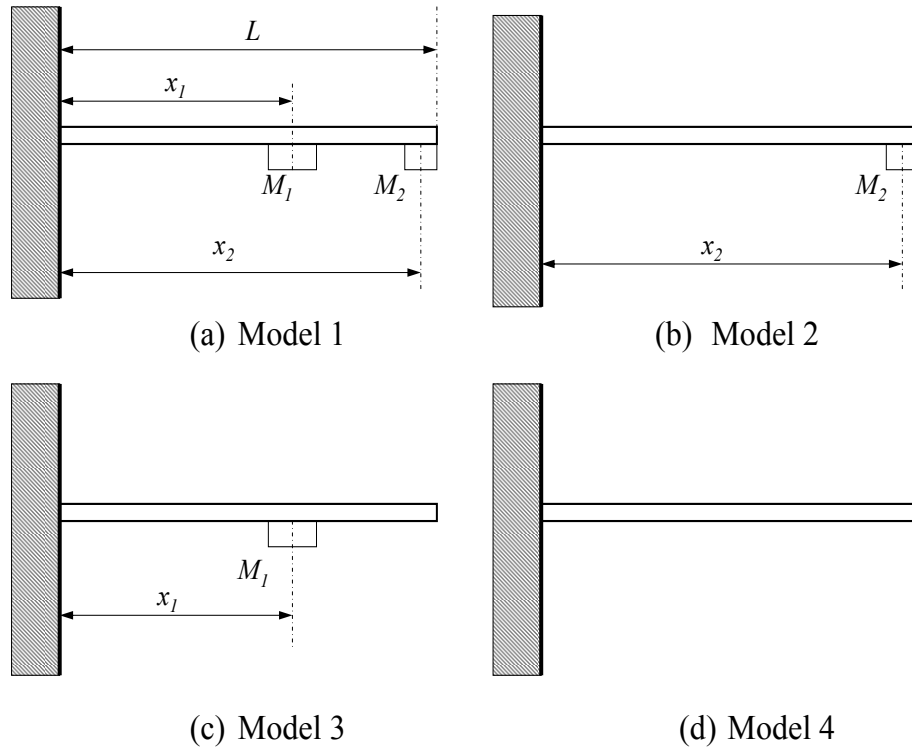


Figure 2.2. Loading model configurations.

signal to each model. The amplitude of the vibration is then measured against the frequency of the signal. The frequencies where the amplitude of vibration forms a peak are the natural frequencies of the models. In the experiments, a sweep signal from a signal generator is amplified using an in-house built piezo power amplifier, and the output from the amplifier is applied to the piezoactuator. The maximum output from the piezosensor is of the order of 500 volts. The piezosensor's output is attenuated by 100 using a differential probe, HZ115 from Hameg InstrumentsTM. The attenuation is necessary in order to make the signal level suitable for input to the analog-to-digital converter. Experiments show that the dominant modes for all the experimental models are the first three modes. The frequencies for the first three modes are shown in Table 2.3.

The table shows that frequencies for the first mode of all four experimental models are separated by more than one decade from their corresponding third mode frequencies. This confirms that the experimental plant is wide-band, which

Model	Natural frequency (Hz)
1	6 44.8 132.7
2	7.1 53.7 155.1
3	8.1 59.4 147.5
4	10.5 64 174

Table 2.3: The first three natural frequencies of the experimental models.

is one of the requirements for the plant used in this research. It is also observed that the added loads make the first three natural frequencies decrease by as much as 43.4%, 30.0%, and 27.0%, respectively. The changes to the frequency response as the model changes are shown in Fig. 2.3. From the figure it can be seen that the added loads not only change the natural frequencies but also change the magnitudes of the vibration at each natural frequency. The figure also reveals the highly resonant characteristic of the flexible structure.

In the next section analytical models of the experimental model will be derived.

2.3 Analytical Model

Two steps are used in building an analytical model of vibrating structures: (i) formulating the physical dynamics of the plant, and (ii) finding the solution of the dynamic formulation. The dynamics of the plant are formulated in the language of mathematics to form equations of motion, which for distributed parameter systems such as flexible beams are typically given in the form of a PDE. To solve

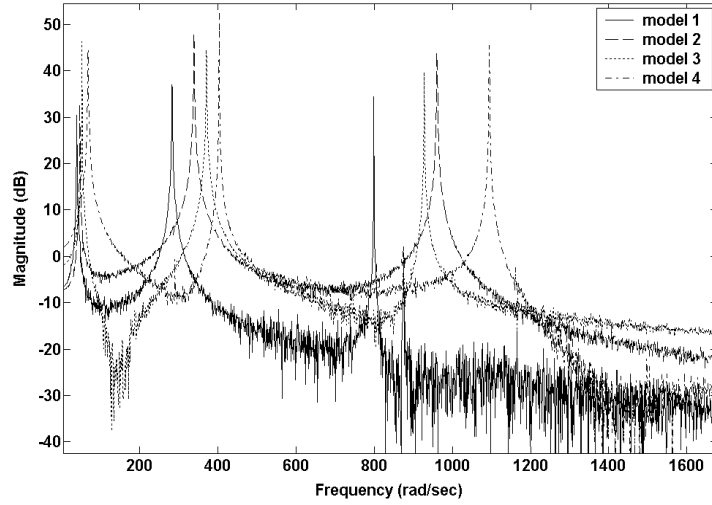


Figure 2.3: Change of frequency responses for various loading conditions.

this PDE, two analytical methods, the modal approach and the wave approach, are commonly used [27]. All the proposed control methods considered in this research are based on modal control. Therefore, to obtain suitable models for the proposed modal-based controllers, the modal approach is used to solve the PDE for the experimental models.

This section is divided into two subsections. In the first subsection, an equation of motion for flexural vibration in a cantilever beam is derived. In the second subsection, modal analysis is used to find the solution of the equation of motion.

2.3.1 Flexural Vibration of Beams

Flexural vibration can occur in many structures such as aircraft wings, robot manipulators, bridges and buildings. In structures where the thickness is relatively small compared to the length and width, flexural vibration is usually more critical to structural integrity than other vibration such as axial vibration and torsional vibration [35]. In the experimental plant, the cantilever beam that is used is thin and relatively long. Hence the torsional and axial vibration in this structure

is negligible compared to the flexural vibration. The research here is concerned with controlling the flexural vibration of the structure. Hence, the equation of motion derived here is only for the flexural vibration.

Consider a thin beam of length L with cross-sectional area A , as shown in Fig. 2.4, whose density and flexural rigidity at point x are $\rho(x)$ and $EI(x)$, respectively. The distributed transverse force is $f(x, t)$. The following assumptions are valid for the beam:

1. The material follows Hooke's Law.
2. The shear deformation is negligible compared to the bending deformation.
3. The rotation of the element is negligible compared to the vertical/transverse translation.

The free-body diagram of an element dx is shown in Fig. 2.5, where Q denotes the shearing force and M the bending moment. Applying Newton's second law to vertical force components (y direction) gives

$$\left(Q(x, t) + \frac{\partial Q(x, t)}{\partial x} dx \right) - Q(x, t) + f(x, t) dx = \rho A(x) dx \frac{\partial^2 y(x, t)}{\partial t^2} \quad (2.1)$$

which is equivalent to

$$\frac{\partial Q(x, t)}{\partial x} + f(x, t) = \rho A(x) \frac{\partial^2 y(x, t)}{\partial t^2}. \quad (2.2)$$

The moment equation of motion about the axis normal to x and y (out-of-the page direction) is

$$\begin{aligned} \left(M(x, t) + \frac{\partial M(x, t)}{\partial x} dx \right) - M(x, t) + \left(Q(x, t) + \frac{\partial Q(x, t)}{\partial x} dx \right) dx \\ + f(x, t) dx \frac{dx}{2} = 0. \end{aligned} \quad (2.3)$$

The terms involving the second power in dx are negligible. Cancelling $M(x, t)$ in (2.3) and disregarding the terms involving the second power in dx , the shearing

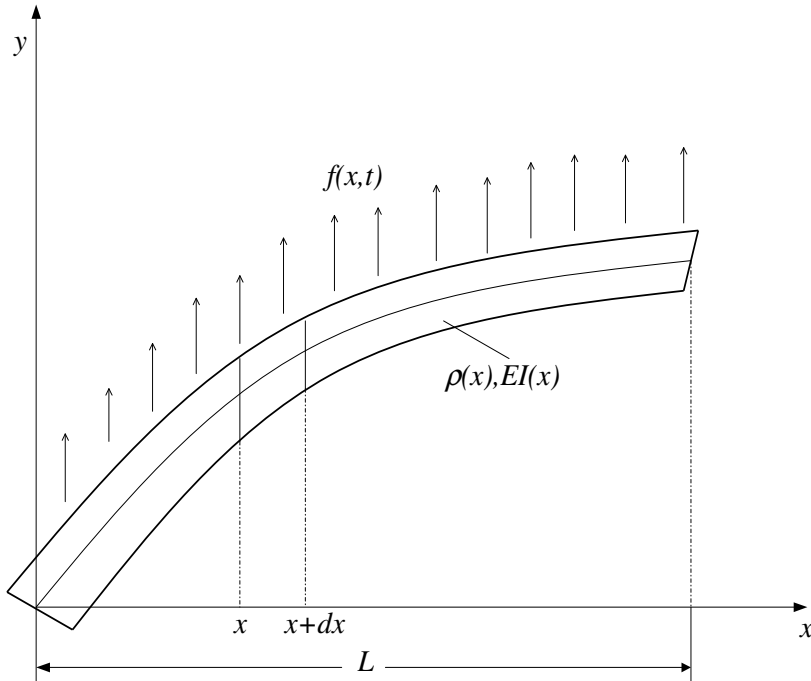


Figure 2.4. A beam in flexural vibration.

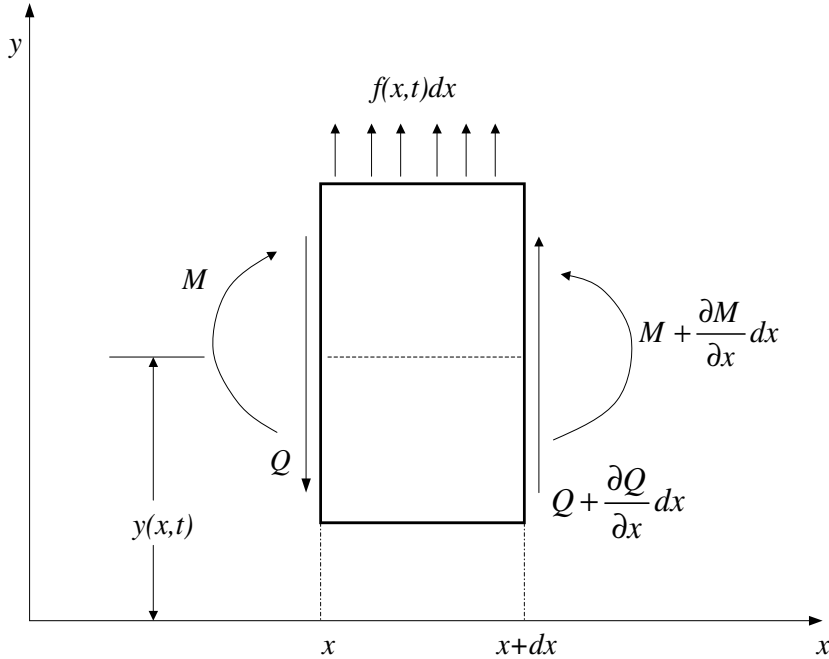


Figure 2.5. A small element of the beam.

force in terms of the bending moment is

$$Q(x, t) = -\frac{\partial M(x, t)}{\partial x}. \quad (2.4)$$

Using the relation from (2.4), (2.2) becomes

$$-\frac{\partial^2 M(x, t)}{\partial x^2} + f(x, t) = \rho A(x) \frac{\partial^2 y(x, t)}{\partial t^2}. \quad (2.5)$$

From the theory of beam bending, the bending moment can be related to the deflection as [120]

$$M(x, t) = EI(x) \frac{\partial^2 y(x, t)}{\partial x^2}. \quad (2.6)$$

By inserting (2.6) into (2.5), the equation of motion for the forced flexural vibration could be described as

$$\frac{\partial^2}{\partial x^2} \left(EI(x) \frac{\partial^2 y(x, t)}{\partial x^2} \right) + \rho A(x) \frac{\partial^2 y(x, t)}{\partial t^2} = f(x, t). \quad (2.7)$$

The experimental plant is a uniform beam. Therefore, (2.7) can be simplified to

$$EI \frac{\partial^4 y(x, t)}{\partial x^4} + \rho A \frac{\partial^2 y(x, t)}{\partial t^2} = f(x, t). \quad (2.8)$$

The PDE (2.8) describes the deflection of the beam $y(x, t)$ for different positions x at different times t . To find a unique solution for $y(x, t)$ from (2.8), two initial conditions and four boundary conditions are needed. The boundary conditions for the models of the experimental plant in this research are [120]

- Fixed at the left end ($x = 0$): The deflection and the slope of the deflection at the left end are zero.

$$\begin{aligned} y(0, t) &= 0, \\ \frac{\partial y(0, t)}{\partial x} &= 0. \end{aligned} \quad (2.9)$$

- Free at the right end ($x = L$): The shearing force and the bending moment at the right end are zero.

$$\begin{aligned}
EI \frac{\partial^2 y(L, t)}{\partial x^2} &= 0, \\
\frac{\partial}{\partial x} \left(EI \frac{\partial^2 y(x, t)}{\partial x^2} \right) \Big|_{(L, t)} &= 0.
\end{aligned} \tag{2.10}$$

- A mass (M) attached at the right end ($x = L$): The shearing force at the right end is zero, the bending moment at the right end is equal to the tensile force caused by the lumped mass (M).

$$\begin{aligned}
EI \frac{\partial^2 y(L, t)}{\partial x^2} &= 0, \\
\frac{\partial}{\partial x} \left(EI \frac{\partial^2 y(x, t)}{\partial x^2} \right) \Big|_{(L, t)} &= M \frac{\partial^2 y(L, t)}{\partial t^2}.
\end{aligned} \tag{2.11}$$

To find the solution of PDE (2.8) for all the experimental models, modal analysis is used.

2.3.2 Modal Analysis

Modal analysis can be used to solve the PDE that describes the equation of motion of a structure [27, 45, 66, 91, 92]. The solution is obtained by first solving the eigenvalue problem for the PDE to produce a set of orthogonal functions known as eigenfunctions. The eigenfunctions are the basis functions used to describe the dynamics of the structure. The orthogonality of the eigenfunctions allows one to replace the PDE with the superposition of an infinite number of decoupled second-order ordinary differential equations (ODE). Each decoupled ODE represents the motion of the structure for a specific mode of vibration, which is characterized in terms of a natural frequency, mode shape, and damping. To find the natural frequency of the structure, a frequency equation is generated from the eigenfunctions and the boundary conditions. Two methods that are widely used to find the frequency equation are the frequency determinant method and the Laplace transforms method [85, 86]. While the mode shape and natural frequency can be found either analytically or experimentally, the damping parameter can

only be found experimentally [45]. Modal analysis is used here to find analytical models for the experimental plant. To find the frequency equation, the frequency determinant method is used.

Consider the typical PDE for flexible structures

$$\mathcal{L}[y(x, t)] + \mathcal{C}\left[\frac{\partial y(x, t)}{\partial t}\right] + \mathcal{M}\left[\frac{\partial^2 y(x, t)}{\partial t^2}\right] = f(x, t). \quad (2.12)$$

\mathcal{L} and \mathcal{M} are linear homogeneous differential operators of order $2p$ and $2q$ respectively and $q \leq p$. Here, x is the spatial coordinate, which is defined over a domain \mathcal{D} . The general arbitrary input is denoted by f , which is distributed over \mathcal{D} . The boundary conditions corresponding to PDE (2.12) can be expressed as

$$\mathcal{B}_i[y(x, t)] = 0, \quad i = 1, 2, \dots, p \quad (2.13)$$

where \mathcal{B}_i is a linear homogeneous differential operator of order less than or equal to $2p - 1$.

In many practical structures, it is sufficiently accurate to assume proportional damping for the purposes of estimating the natural frequencies and mode shapes of the structures [45]. Proportional damping is a special type of damping where the damping matrix is proportional to the mass and stiffness matrices. By assuming proportional damping, \mathcal{C} can be defined as a linear combination of the mass and stiffness operators, \mathcal{L} and \mathcal{M}

$$\mathcal{C} = c_1\mathcal{L} + c_2\mathcal{M}, \quad (2.14)$$

where c_1 and c_2 are non-negative constants. The advantage of using proportional damping is that the mode shapes (eigenfunctions) for both the damped and undamped cases are the same and the natural frequencies (eigenvalues) are also very similar [45]. Therefore, the eigenfunctions $y_m(x)$ can be obtained by solving the eigenvalue problem associated with undamped version of (2.12)

$$\mathcal{L}[y_m(x)] = \lambda_m\mathcal{M}[y_m(x)], \quad m = 1, 2, \dots \quad (2.15)$$

and its associated boundary conditions (2.13). The natural frequencies ω_m are determined from the eigenvalues

$$\lambda_m = \omega_m^2. \quad (2.16)$$

To be used as the basis function to find the solution of PDE (2.12), the eigenfunctions need to be orthogonal. To develop the general principle of orthogonality, define the self-adjoint eigenvalue problem. For any two arbitrary eigenfunctions $y_m(x)$ and $y_n(x)$, the eigenvalue problem is self-adjoint if [27]

$$\int_D y_m(x) \mathcal{L}[y_n(x)] dD(x) = \int_D y_n(x) \mathcal{L}[y_m(x)] dD(x) \quad (2.17)$$

and

$$\int_D y_m(x) \mathcal{M}[y_n(x)] dD(x) = \int_D y_n(x) \mathcal{M}[y_m(x)] dD(x). \quad (2.18)$$

Now, let ω_m^2 and ω_n^2 be two distinct eigenvalues with corresponding eigenfunctions $y_m(x)$ and $y_n(x)$ resulting from the solution of the self-adjoint eigenvalue problem. Then the generalized condition of the orthogonality equation can be obtained as

$$\int_D y_m(x) \mathcal{M}[y_n(x)] dD(x) = 0, \quad \text{for } \omega_m^2 \neq \omega_n^2. \quad (2.19)$$

From the eigenvalue problem, it follows that

$$\int_D y_m(x) \mathcal{L}[y_n(x)] dD(x) = 0, \quad \text{for } \omega_m^2 \neq \omega_n^2. \quad (2.20)$$

For simplicity, the eigenfunctions are typically normalized with respect to \mathcal{M} such that

$$\int_D y_m(x) \mathcal{M}[y_n(x)] dD(x) = \delta_{mn}, \quad (2.21)$$

where δ_{mn} is the Kronecker delta function, where $\delta_{mn} = 1$ for $m = n$, and zero otherwise. Thus, (2.20) can be written as

$$\int_D y_m(x) \mathcal{L}[y_n(x)] dD(x) = \delta_{mn} \omega_m^2. \quad (2.22)$$

Since proportional damping is assumed,

$$\int_D y_m(x) \mathcal{C} [w_n(x)] dD(x) = c_1 \delta_{mn} \omega_m^2 + c_2 \delta_{mn} \quad (2.23)$$

which can be written as

$$\int_D y_m(x) \mathcal{C} [w_n(x)] dD(x) = \delta_{mn} 2\zeta_m \omega_m \quad (2.24)$$

with

$$\zeta_m = \frac{1}{2\omega_m} (c_1 \omega_m^2 + c_2) \quad (2.25)$$

where ζ_m is damping ratio of the mode m . Equations (2.21), (2.22), and (2.24) are orthonormal eigenfunctions which form a basis that span the solution space of the eigenvalue problem. Thus, the response of the system can be computed at any arbitrary point in the domain \mathcal{D} as a superposition of these basis functions [27]

$$y(x, t) = \sum_{m=1}^{\infty} y_m(x) q_m(t), \quad (2.26)$$

where $q_m(t)$ are the generalized coordinates.

To solve PDE (2.12) using modal analysis, substituting (2.26) into (2.12), one obtains

$$\begin{aligned} \mathcal{L} \left[\sum_{m=1}^{\infty} y_m(x) q_m(t) \right] + \mathcal{C} \left[\frac{\partial}{\partial t} \sum_{m=1}^{\infty} y_m(x) q_m(t) \right] \\ + \mathcal{M} \left[\frac{\partial^2}{\partial t^2} \sum_{m=1}^{\infty} y_m(x) q_m(t) \right] = f(x, t). \end{aligned} \quad (2.27)$$

Multiplying (2.27) by $y_n(x)$ and integrating over the domain D , gives

$$\sum_{m=1}^{\infty} q_m(t) \delta_{mn} \omega_m^2 + \sum_{m=1}^{\infty} \dot{q}_m(t) \delta_{mn} 2\zeta_m \omega_m + \sum_{m=1}^{\infty} \ddot{q}_m(t) \delta_{mn} = Q_n(t) \quad (2.28)$$

where

$$Q_n(t) = \int_D y_n(x) f(x, t) dD(x) \quad (2.29)$$

is defined as the n^{th} generalized force. Taking advantage of the orthogonality conditions (2.22), (2.21) and (2.24), the summation in (2.28) only holds when

$m = n$. Thus, one obtains an infinite set of uncoupled ordinary differential equations

$$\ddot{q}_m(t) + 2\zeta_m\omega_m\dot{q}_m(t) + \omega_m^2q_m(t) = Q_m(t), \quad m = 1, 2, \dots \quad (2.30)$$

From (2.30) it can be seen that the system is described by an infinite set of second-order differential equations that can be solved independently.

In control design, due to the versatility of the frequency domain method, the frequency domain model is often required. The solution to each second-order differential equation in the frequency domain can be found using Laplace transforms. In many cases, the generalized force Q_m can be written as a decomposition of the spatial and temporal components [96]

$$Q_m(t) = P_m u(t), \quad (2.31)$$

where $u(t)$ is the input to the system and P_m is the time-independent forcing term. Taking the Laplace transform of the second-order equation (2.30), the transfer function of the system can be shown to be

$$G(s, x) = \sum_{m=1}^{\infty} \frac{y_m(x)P_m}{s^2 + 2\zeta_m\omega_m s + \omega_m^2}. \quad (2.32)$$

Equation (2.32) is an infinite-dimensional transfer function due to the existence of an infinite number of modes. This is a general solution for PDE (2.12). The solution for a particular structure is then solved by finding the eigenfunction (y_m), the natural frequency (ω_m), and the structural damping (ζ_m). The solutions for the experimental models are now discussed. The solution for the cantilever beam without loads is solved first, followed by the solution for the cantilever beam with loads located at arbitrary positions along the beam. In finding the solutions the following assumptions are made:

1. The beam is perfectly clamped to the concrete.

2. The effects of the cables connected to the magnetically clamped loads on the dynamics of the structure can be ignored.
3. The masses of the piezoceramic patches are negligible compared to the mass of the beam and the masses of the loads, thus the loading effects of the piezoceramic patches on the dynamics of the structure can be ignored.
4. The placement of the loads are accurately positioned and the loads are perfectly clamped to the beam.

Solution for a cantilevered beam

Consider a cantilevered uniform beam of length L where a point force u is acting at point $x = x_1$ as shown in Fig. 2.6. For a linear system, such as the experimental plant in this research, the solution for general excitation can be obtained from the solution with a point force. The PDE that describes the dynamics of the beam is (2.8), and the boundary conditions are described as in (2.9) and (2.10). For a uniform beam the boundary conditions in (2.9) and (2.10) can be written as

$$\begin{aligned}
 y(0) &= 0, \\
 \left. \frac{dy(x)}{dx} \right|_{x=0} &= 0, \\
 \left. \frac{d^2y(x)}{dx^2} \right|_{x=L} &= 0, \\
 \left. \frac{d^3y(x)}{dx^3} \right|_{x=L} &= 0.
 \end{aligned} \tag{2.33}$$

Comparing the general notations in (2.12) and (2.13) with the notations in (2.8) and (2.33) one obtains

$$\begin{aligned}
 \mathcal{L} &= EI \frac{\partial^4}{\partial x^4}, \\
 \mathcal{M} &= \rho A, \\
 &\vdots
 \end{aligned}$$

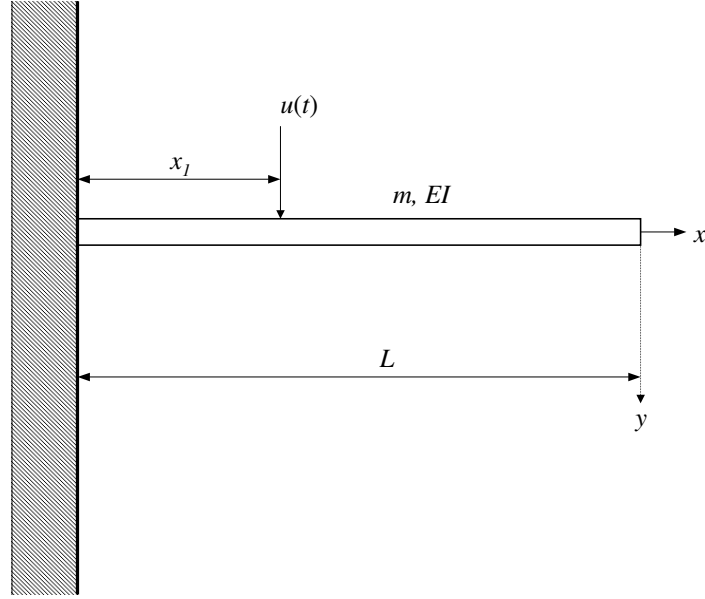


Figure 2.6. A cantilever beam.

$$\begin{aligned}
 \mathcal{B}_1 &= 1, \\
 \mathcal{B}_2 &= EI \frac{\partial^2}{\partial x^2} \\
 f(x, t) &= u(t) \delta(x - x_1)
 \end{aligned} \tag{2.34}$$

and $\mathcal{D} = [0, L]$. \mathcal{C} is defined as in (2.14) to include damping in the structure.

Using (2.34), the orthogonality conditions (2.21) and (2.22) can be written as

$$\int_0^L y_m(x) y_n(x) \rho A dx = \delta_{mn}, \tag{2.35}$$

$$\int_0^L y_m(x) y_n''''(x) EI dx = \delta_{mn} \omega_m^2, \tag{2.36}$$

where y_m and ω_m are the solutions to the eigenvalue problem (2.15). The general solution to the eigenvalue problem (2.15) is [27, 120]

$$y_m(x) = C_{1m} \cos \beta_m x + C_{2m} \sin \beta_m x + C_{3m} \cosh \beta_m x + C_{4m} \sinh \beta_m x, \tag{2.37}$$

where

$$\beta_m^4 = \frac{\rho A \omega_m^2}{EI} \tag{2.38}$$

and C_{1m} , C_{2m} , C_{3m} and C_{4m} are constants. The constants C_{1m} , C_{2m} , C_{3m} and C_{4m} can be found from the boundary conditions.

To find the frequency equation for the cantilevered beam, apply the frequency determinant method to the eigenfunctions (2.37) and the boundary conditions (2.33). Dropping the subscript m in (2.37) to simplify the notation, and substituting it into the first and the second rows of (2.33) yields

$$\begin{aligned} y(0) = 0 &= C_1 + C_3, \\ \left. \frac{dy(x)}{dx} \right|_{x=0} &= 0 = \beta(C_2 + C_4). \end{aligned} \quad (2.39)$$

Using results from (2.39), (2.37) can be simplified to

$$y(x) = C_1(\cos \beta x - \cosh \beta x) + C_2(\sin \beta x - \sinh \beta x). \quad (2.40)$$

Substituting (2.40) into the third and fourth rows of (2.33), results in the following two homogeneous equations

$$\begin{aligned} \left. \frac{d^2 y(x)}{dx^2} \right|_{x=L} &= 0 \\ &= -\beta^2 \times [C_1(\cos \beta L + \cosh \beta L) + C_2(\sin \beta L + \sinh \beta L)], \end{aligned} \quad (2.41)$$

and

$$\begin{aligned} \left. \frac{d^3 y(x)}{dx^3} \right|_{x=L} &= 0 \\ &= -\beta^3 \times [C_1(\sinh \beta L - \sin \beta L) + C_2(\cos \beta L + \cosh \beta L)]. \end{aligned} \quad (2.42)$$

For a nontrivial solution of C_1 and C_2 from (2.41) and (2.42), the determinant of their coefficients must be zero, i.e.,

$$\begin{vmatrix} (\cos \beta L + \cosh \beta L) & (\sin \beta L + \sinh \beta L) \\ \beta(\sinh \beta L - \sin \beta L) & \beta(\cos \beta L + \cosh \beta L) \end{vmatrix} = 0. \quad (2.43)$$

Solving the determinant gives the frequency equation

$$\cos \beta L \cosh \beta L = -1. \quad (2.44)$$

The roots $\beta_m L$ are found by inserting the subscript m into β in (2.44) and solving (2.44). Applying $\beta_m L$ into (2.38), gives the natural frequency of vibration

$$\omega_m = (\beta_m L)^2 \sqrt{\frac{EI}{\rho AL^4}}, \quad m = 1, 2, \dots \quad (2.45)$$

Furthermore, solving (2.41) for C_2 in terms of C_1 and substituting it into (2.40), the equation of modes shapes is obtained as

$$y_m(x) = C_m \times \left[(\sin \beta_m x - \sinh \beta_m x) - \frac{(\sin \beta_m L + \sinh \beta_m L)}{(\cos \beta_m L + \cosh \beta_m L)} (\cos \beta_m x - \cosh \beta_m x) \right]. \quad (2.46)$$

The coefficient C_m can be obtained by substituting (2.46) into the orthogonality conditions (2.35) and (2.36). After finding the eigenfunction (y_m) and the natural frequencies (ω_m), introduce damping into the system, where ζ_m denotes the damping ratio associated with mode m . Then following (2.32), the transfer function from the applied force $U(s)$ to the transverse deflection of the beam $Y(s, x)$ is found to be

$$\frac{Y(s, x)}{U(s)} = \sum_{m=1}^{\infty} \frac{y_m(x)y_m(x_1)}{s^2 + 2\zeta_m\omega_m s + \omega_m^2} \quad (2.47)$$

where $y_m(x)$ and $y_m(x_1)$ are the m^{th} eigenfunctions at the degrees of freedom x and x_1 respectively.

Solution for a cantilevered beam with attached masses at arbitrary positions

The analysis of a beam carrying multiple concentrated masses has been of interest to researchers since the late sixties [10, 80, 83, 84, 85, 86, 139]. This is due to the fact that the problem of a beam carrying concentrated masses is widely found

in engineering applications such as robotics, aerospace, railway bridges and long highway bridges. Analytical methods and numerical methods can be used to obtain the natural frequencies of beam structures. Stanišić and Hardin [139] developed a method based on Fourier analysis to solve the natural frequencies of a simply supported beam carrying a moving mass. The equation of motion is given in terms of δ -dirac functions and is solved through the use of the first term Fourier finite sine and cosine series. Due to the use of the first term series approximation only, this method gives inaccurate results. Approximation using higher terms can only be solved numerically because the solution is not in a closed form. Other methods use the Laplace transform [36, 80] and a combined analytical and numerical method [151]. In the Laplace transform method, the effect of the attached masses is expressed by the use of δ -dirac function and the equation of motion is derived by using the Timoshenko or Euler-Bernoulli beam theories. The differential equation is then solved by means of the Laplace transform method. In the combined analytical-numerical method the eigenvalue equation is derived analytically and then the eigenvalues and eigenfunctions are calculated numerically. Low [83, 84, 85, 86] has done extensive research on the vibration analysis of beams carrying concentrated masses at arbitrary locations. He compared the effectiveness of the Laplace transform method and the frequency determinant method to generate the eigenfrequency equation of a beam carrying multiple concentrated masses at arbitrary positions. He also compared the results from the analytical method and numerical method using Rayleigh's method and he concluded that the solution obtained using the frequency determinant method can be obtained faster than by using the Laplace transform method [85], and that the Rayleigh's numerical method gives a good approximation to the analytical method with the advantage of a saving in computation time.

From the above discussion, it can be concluded that the combination of analytical and numerical methods is the best way to find the natural frequencies of

a beam carrying concentrated masses at arbitrary positions along the beam. In this research, the frequency equation of the system is derived analytically using the frequency determinant method, and the natural frequencies of the system are determined numerically. Due to the complexity of the equations, the MatlabTM symbolic mathematics toolbox is used to derive the frequency equations of the systems, and the natural frequencies are found numerically and/or graphically using Matlab.

Consider a cantilever beam of mass m carrying n concentrated masses M_1 to M_n at arbitrary positions as shown in Fig. 2.7. The beam is assumed to be segmented into $n + 1$ segments. The general solutions of the eigenvalue problem for the loaded beam system are as in (2.37). To simplify the notation drop the subscript m and define the solution for different segments as

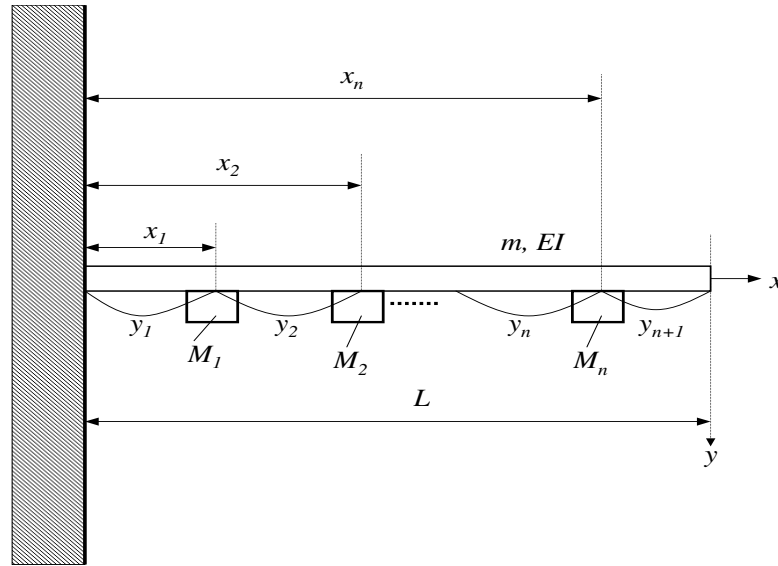


Figure 2.7. A cantilever beam with n attached masses.

$$\begin{cases} y_1(x) = C_1 \cos \beta x + C_2 \sin \beta x + C_3 \cosh \beta x + C_4 \sinh \beta x, \\ y_2(x) = C_5 \cos \beta x + C_6 \sin \beta x + C_7 \cosh \beta x + C_8 \sinh \beta x, \\ \vdots \\ y_{n+1}(x) = C_{4(n+1)-3} \cos \beta x + C_{4(n+1)-2} \sin \beta x + \\ \quad C_{4(n+1)-1} \cosh \beta x + C_{4(n+1)} \sinh \beta x, \end{cases} \quad (2.48)$$

where C_1 to $C_{4(n+1)}$ are constants to be determined, and y_1 to y_{n+1} are the transverse displacements associated with the respective concentrated masses M_1 to M_n . The compatibility conditions at the locations of n concentrated masses are given as follows [86]

$$\begin{cases} y_1(x_1) = y_2(x_1), \\ y_1'(x_1) = y_2'(x_1), \\ y_1''(x_1) = y_2''(x_1), \\ y_1'''(x_1) - y_2'''(x_1) + \alpha_1\beta^4 y_1(x_1) = 0, \end{cases}$$

$$\begin{cases} y_2(x_2) = y_3(x_2), \\ y_2'(x_2) = y_3'(x_2), \\ y_2''(x_2) = y_3''(x_2), \\ y_2'''(x_2) - y_3'''(x_2) + \alpha_2\beta^4 y_2(x_2) = 0, \end{cases}$$

$$\vdots$$

$$\begin{cases} y_n(x_n) = y_{n+1}(x_n), \\ y_n'(x_n) = y_{n+1}'(x_n), \\ y_n''(x_n) = y_{n+1}''(x_n), \\ y_n'''(x_n) - y_{n+1}'''(x_n) + \alpha_n\beta^4 y_n(x_n) = 0, \end{cases}$$
(2.49)

where

$$\alpha_i = \frac{M_i}{m}, \quad i = 1, 2, \dots, n \quad (2.50)$$

is the corresponding mass ratio. The boundary conditions for a cantilever beam are as in (2.9) and (2.10) and can be written as

$$\begin{aligned} y_1(0) &= 0, \\ y_1'(0) &= 0, \\ y_{n+1}''(L) &= 0, \\ y_{n+1}'''(L) &= 0. \end{aligned} \quad (2.51)$$

There are $4(n+1)$ constants, C_1 to $C_{4(n+1)}$ in (2.48), $4n$ equations in (2.49) and 4 equations in (2.51). Substituting (2.48) into (2.49) and (2.51) results in $4(n+1)$ equations with $4(n+1)$ constants which can be written as

$$\mathbf{BC} = \mathbf{0}, \quad (2.52)$$

where $\mathbf{C} = \{C_1, C_2, \dots, C_{4(n+1)}\}^T$ and \mathbf{B} is the associated $4(n+1) \times 4(n+1)$ matrix. For a non trivial solution of C_1 to $C_{4(n+1)}$, the determinant of their coefficient must be zero i.e.,

$$|\mathbf{B}| = 0. \quad (2.53)$$

Solving the determinant (2.53) gives the frequency equation. The eigenvalues which are associated with the natural frequencies can be found by solving the generated frequency equation. The maximum number of loads attached to the cantilever beam in the experimental plant is two. Therefore, only the frequency equations for a cantilever beam with one and two loads at arbitrary positions are derived in this section.

Solution a for cantilevered beam with one attached mass

For only one mass M attached to the cantilever beam, the beam is considered as being split into two segments y_1 and y_2 with the general solution

$$\begin{aligned} y_1(x) &= C_1 \cos \beta x + C_2 \sin \beta x + C_3 \cosh \beta x + C_4 \sinh \beta x, \\ y_2(x) &= C_5 \cos \beta x + C_6 \sin \beta x + C_7 \cosh \beta x + C_8 \sinh \beta x. \end{aligned} \quad (2.54)$$

The compatibility conditions at the location of the concentrated mass are

$$y_1(x_1) = y_2(x_1), \quad (2.55)$$

$$y_1'(x_1) = y_2'(x_1), \quad (2.56)$$

$$y_1''(x_1) = y_2''(x_1), \quad (2.57)$$

$$y_1'''(x_1) - y_2'''(x_1) + \alpha_1 \beta^4 y_1(x_1) = 0. \quad (2.58)$$

The boundary conditions are

$$y_1(0) = 0, \quad (2.59)$$

$$y_1'(0) = 0, \quad (2.60)$$

$$y_2''(L) = 0, \quad (2.61)$$

$$y_2'''(L) = 0. \quad (2.62)$$

Substituting $y_1(x)$ from (2.54) to (2.59) gives

$$C_1 + C_3 = 0. \quad (2.63)$$

Deriving $y_1(x)$ in (2.54) once against x and substituting the results into (2.60) gives

$$\beta C_2 + \beta C_4 = 0. \quad (2.64)$$

Substituting the second derivative of $y_2(x)$ against x in (2.54) into (2.61) gives

$$-C_5\beta^2 \cos \beta L - C_6\beta^2 \sin \beta L + C_7\beta^2 \cosh \beta L + C_8\beta^2 \sinh \beta L = 0. \quad (2.65)$$

Substituting the third derivative of $y_2(x)$ against x in (2.54) into (2.62) gives

$$C_5\beta^3 \sin \beta L - C_6\beta^3 \cos \beta L + C_7\beta^3 \sinh \beta L + C_8\beta^3 \cosh \beta L = 0. \quad (2.66)$$

Substituting (2.54) into (2.55), (2.56), (2.57) and (2.58) gives the following equations

$$\begin{aligned} & C_1 \cos \beta x_1 + C_2 \sin \beta x_1 + C_3 \cosh \beta x_1 + C_4 \sinh \beta x_1 \\ & -C_5 \cos \beta x_1 - C_6 \sin \beta x_1 - C_7 \cosh \beta x_1 - C_8 \sinh \beta x_1 = 0, \end{aligned} \quad (2.67)$$

$$\begin{aligned} & -C_1\beta \sin \beta x_1 + C_2\beta \cos \beta x_1 + C_3\beta \sinh \beta x_1 + C_4\beta \cosh \beta x_1 \\ & +C_5\beta \sin \beta x_1 - C_6\beta \cos \beta x_1 - C_7\beta \sinh \beta x_1 - C_8\beta \cosh \beta x_1 = 0, \end{aligned} \quad (2.68)$$

$$\begin{aligned} & -C_1\beta^2 \cos \beta x_1 - C_2\beta^2 \sin \beta x_1 + C_3\beta^2 \cosh \beta x_1 + C_4\beta^2 \sinh \beta x_1 \\ & +C_5\beta^2 \cos \beta x_1 + C_6\beta^2 \sin \beta x_1 - C_7\beta^2 \cosh \beta x_1 - C_8\beta^2 \sinh \beta x_1 = 0, \end{aligned} \quad (2.69)$$

$$\begin{aligned} & C_1 [\beta^3 \sin \beta x_1 + \alpha\beta^4 \cos \beta x_1] + C_2 [\alpha\beta^4 \sin \beta x_1 - \beta^3 \cos \beta x_1] \\ & +C_3 [\beta^3 \sinh \beta x_1 + \alpha\beta^4 \cosh \beta x_1] + C_4 [\beta^3 \cosh \beta x_1 + \alpha\beta^4 \sinh \beta x_1] \\ & -C_5\beta^3 \sin \beta x_1 + C_6\beta^3 \cos \beta x_1 - C_7\beta^3 \sinh \beta x_1 - C_8\beta^3 \cosh \beta x_1 = 0. \end{aligned} \quad (2.70)$$

Using (2.63) to (2.70), (2.52) can be formed with \mathbf{B} of dimension 8×8 . Solving the $\det(\mathbf{B}) = 0$ using MatlabTM symbolic mathematics toolbox, gives the frequency equation as follows

$$\begin{aligned}
& 2\alpha\beta \cosh \beta x_1 \sin \beta x_1 - 2\beta \cos \beta x_1 \alpha \sinh \beta x_1 + \\
& 2\beta\alpha \sin \beta(-L + x_1) \cosh \beta(-L + x_1) - 2\beta\alpha \cos \beta(-L + x_1) \sinh \beta(-L + x_1) - \\
& \beta\alpha \sinh \beta L \cos \beta(-L + 2x_1) + \beta\alpha \sin \beta L \cosh \beta(-L + 2x_1) + \\
& \beta\alpha \sin \beta L \cosh \beta L - \beta\alpha \cos \beta L \sinh \beta L - 4 \cos \beta L \cosh \beta L - 4 = 0.
\end{aligned} \tag{2.71}$$

Equation (2.71) is the frequency equation for a cantilever beam with a load at arbitrary position (x_1) along the beam. The validity of this equation needs to be checked prior to the application of the equation to find the natural frequencies of the system. This is done by making comparisons against known valid models using a comparison technique [128]. The two valid frequency equations available from the literature are frequency equation for a cantilever beam without load [92, 120] which is (2.44), and the frequency equation for a cantilever beam with a load at the tip of the beam [71, 92]

$$\alpha\beta \sin \beta L \cosh \beta L - \alpha\beta \cos \beta L \sinh \beta L - \cos \beta L \cosh \beta L - 1 = 0. \tag{2.72}$$

To compare frequency equation (2.71) against the two valid frequency equations (2.44) and (2.72), the parameters α and x_1 in (2.71) need to be set properly. To compare frequency equation (2.71) against the frequency equations of a beam without load (2.44), set $\alpha = 0$ in (2.71). By setting $\alpha = 0$ in (2.71) frequency equation (2.44) is obtained. To compare the frequency equation (2.71) against the frequency equations of a beam with load at the tip of the beam (2.72) set $x_1 = L$ in (2.71). By setting $x_1 = L$ in (2.71) frequency equation (2.72) is obtained. Therefore, from the comparisons with two different valid frequency equations (2.44) and (2.72), it can be seen that the frequency equation (2.71) is

valid. The natural frequencies of a beam with a load at an arbitrary position can then be found using frequency equation (2.71).

Solution for cantilevered a beam with two attached masses

For two masses M_1 and M_2 attached to the cantilever beam, there are eight compatibility conditions, four boundary conditions and twelve constants (C_1 to C_{12}). Using the same procedure as for a cantilever beam with one mass attached to the cantilever beam, (2.52) can be formed with \mathbf{B} of dimension 12×12 . Solving the $\det(\mathbf{B}) = 0$ using MatlabTM symbolic mathematics toolbox, gives the frequency equation as follows

$$\begin{aligned}
& 16 - 8\alpha_1\beta \cosh \beta x_1 \sin \beta x_1 + \\
& \beta^2 \alpha_1 \alpha_2 \sinh \beta L \sin \beta(L - 2x_2) - \beta^2 \alpha_1 \alpha_2 \cos \beta L \cosh \beta(L - 2x_1) + \\
& \beta^2 \alpha_1 \alpha_2 \sin \beta(L - 2x_1) \sinh \beta(L - 2x_2) - \beta^2 \alpha_1 \alpha_2 \cos \beta L \cosh \beta(L - 2x_2) + \\
& \beta^2 \alpha_1 \alpha_2 \sin \beta(L - 2x_2) \sinh \beta(L - 2x_1) - \beta^2 \alpha_1 \alpha_2 \sin \beta L \sinh \beta(L - 2x_1) - \\
& \beta^2 \alpha_1 \alpha_2 \cos \beta L \cosh \beta(-2x_2 + L + 2x_1) + \beta^2 \alpha_1 \alpha_2 \cosh \beta L \cos \beta(L - 2x_2) - \\
& \beta^2 \alpha_1 \alpha_2 \sinh \beta L \sin \beta(L - 2x_1) + \beta^2 \alpha_1 \alpha_2 \cosh \beta L \cos \beta(-2x_2 + L + 2x_1) + \\
& \beta^2 \alpha_1 \alpha_2 \sin \beta L \sinh \beta(L - 2x_2) + 4\beta \alpha_2 \cos \beta L \sinh \beta L + \\
& \beta^2 \alpha_1 \alpha_2 \cosh \beta L \cos \beta(L - 2x_1) + 16 \cos \beta L \cosh \beta L + \\
& 4\beta^2 \alpha_1 \alpha_2 \sin \beta(-x_1 + L) \sinh \beta(-x_1 + L) + 2\beta^2 \alpha_1 \sin \beta x_2 \alpha_2 \sinh \beta(-x_2 + 2x_1) - \\
& 4\beta \alpha_2 \sin \beta L \cosh \beta L + 2\beta^2 \alpha_1 \alpha_2 \sinh \beta x_2 \sin \beta(-x_2 + 2x_1) - \\
& 2\beta^2 \alpha_1 \alpha_2 \cos \beta(-x_1 + L - x_2) \cosh \beta(x_1 + L - x_2) + \\
& 2\beta^2 \alpha_1 \alpha_2 \cosh \beta x_2 \cos \beta(-x_2 + 2x_1) - \\
& 2\beta^2 \alpha_1 \alpha_2 \cos \beta(-2x_2 + x_1 + L) \cosh \beta(-x_1 + L) + \\
& 2\beta^2 \alpha_1 \alpha_2 \cos \beta(x_1 + L - x_2) \cosh \beta(-x_1 + L - x_2) - \\
& 2\beta^2 \alpha_1 \alpha_2 \sin \beta(-2x_2 + x_1 + L) \sinh \beta(-x_1 + L) + \\
& 2\beta^2 \alpha_1 \alpha_2 \sin \beta(x_1 + L - x_2) \sinh \beta(x_1 + L - x_2) -
\end{aligned}$$

$$\begin{aligned}
& 2\beta^2\alpha_1 \cos \beta x_2 \alpha_2 \cosh \beta(-x_2 + 2x_1) + \\
& 8\beta^2\alpha_1\alpha_2 \sin \beta(-x_2 + x_1) \sinh \beta(-x_2 + x_1) + \\
& 2\beta^2\alpha_1\alpha_2 \cos \beta(-x_1 + L) \cosh \beta(-2x_2 + x_1 + L) - \\
& 2\beta^2\alpha_1\alpha_2 \sin \beta(-x_1 + L) \sinh \beta(-2x_2 + x_1 + L) - \\
& 2\beta^2\alpha_1\alpha_2 \sin \beta(-x_1 + L - x_2) \sinh \beta(-x_1 + L - x_2) - \\
& 2\alpha_1\beta^2\alpha_2 \sin \beta L \sinh \beta L - 4\alpha_1\beta^2 \sin \beta x_2 \alpha_2 \sinh \beta x_2 + \\
& 4\beta\alpha_1 \cos \beta L \sinh \beta L - 4\beta\alpha_1 \sin \beta L \cosh \beta L - 8\beta \sin \beta x_2 \alpha_2 \cosh \beta x_2 + \\
& 8 \cos \beta x_1 \alpha_1 \beta \sinh \beta x_1 + 8\beta \cos \beta x_2 \alpha_2 \sinh \beta x_2 - 4\beta\alpha_2 \sin \beta L \cosh \beta(L - 2x_2) + \\
& 4\beta\alpha_1 \sinh \beta L \cos \beta(L - 2x_1) + 4\beta\alpha_2 \sinh \beta L \cos \beta(L - 2x_2) + \\
& 8\beta\alpha_1 \sin \beta(-x_1 + L) \cosh \beta(-x_1 + L) - 4\beta\alpha_1 \sin \beta L \cosh \beta(L - 2x_1) + \\
& 8\beta\alpha_2 \sin \beta(L - x_2) \cosh \beta(L - x_2) - 8\beta\alpha_1 \cos \beta(-x_1 + L) \sinh \beta(-x_1 + L) - \\
& 8\beta\alpha_2 \cos \beta(L - x_2) \sinh \beta(L - x_2) = 0.
\end{aligned} \tag{2.73}$$

Equation (2.73) is the frequency equation for a cantilever beam with two masses at arbitrary positions (x_1) and (x_2) along the beam. The validity of the frequency equation (2.73) is tested by the same procedure as for the one mass case. The frequency equation (2.71) is now a valid equation, therefore, the validity of (2.73) can be tested by comparing it against (2.71). To compare (2.73) against (2.71), set $\alpha_2 = 0$ in (2.73). Setting $\alpha_2 = 0$ in (2.73) makes all terms in (2.73) except the 1st, 2nd, 16th, 33rd, 34th, 36th, 39th, 41st, 42nd and 44th terms equal to zero. All the ten non-zero terms form an equation which is the same as (2.71). Furthermore, setting $\alpha_1 = \alpha_2 = 0$ in (2.73) results in (2.44) and setting $x_2 = L, \alpha_1 = 0$ in (2.73) results in (2.72). Therefore, comparisons with all the valid frequency equations (2.44), (2.72) and (2.71) show that the frequency equation (2.73) is valid. The natural frequencies of a beam with two masses at arbitrary positions then can be found using frequency equation (2.73).

To find the natural frequencies of all the models in the experimental plant, insert the corresponding parameters values x_1 , x_2 , α_1 and α_2 from Table 2.1 and Table 2.2 into frequency equation (2.73), find the equation roots (β_m) then insert into (2.45). The experiments with the experimental plant show that the most dominant modes for all the different loading conditions are the first three modes. Therefore, only natural frequencies of the first three modes are identified here. The roots (β_m) for each model are found graphically using MatlabTM. It is achieved by plotting the frequency equation (2.73) and finding the values where the graph intercepts the frequency axis. The first three roots (β_m), $m= 1$ to 3 are shown in Table 2.4. From the values of (β_m), the natural frequencies of the

Model	$\beta_m, m = 1-3$
1	1.4477 3.9842 6.8439
2	1.5486 4.3478 7.5599
3	1.6482 4.5595 7.1418
4	1.8749 4.6941 7.8547

Table 2.4. The first three frequency equation's roots of the models.

models can be calculated. The first three natural frequencies of all the models compared to the first three natural frequencies from the experimental results are shown in Table 2.5.

From Table 2.5, it can be seen that the analytical results are very close to the experimental results with the errors ranging from 0.32% for the second natural frequency of Model 2 to 4.82% for the first natural frequency of Model 4.

There are several factors that may cause the discrepancies between the an-

Model	Experimental results (Hz)	Analytical results from (Hz)	error (%)
1	6	5.9726	0.46
	44.8	45.2367	0.97
	132.7	133.48	0.58
2	7.1	6.834	3.89
	53.7	53.8702	0.32
	155.1	162.87	4.77
3	8.1	7.7416	4.63
	59.4	59.2439	0.26
	147.5	145.3532	1.48
4	10.5	10.0176	4.82
	64	62.7934	1.92
	174	175.8200	1.04

Table 2.5: Comparison of natural frequencies obtained from experimental and analytical results.

analytical and experimental results, such as imperfect clamping conditions at the fixed end, imperfect clamping of the loads to the beam, imperfect positioning of the loads, the loading effect of cabling from the magnetically clamped loads, and the loading effect of the piezoceramic patches. These factors are ignored or assumed to be perfect in the four assumptions for finding the solution analytically. The discrepancies, however, are reasonably small (less than 5%). Hence the models are considered to be reasonably accurate for the purpose of the experiments. Furthermore, the proposed controllers are designed to cope with plants with natural frequency variations and unmodeled dynamics. Therefore, in the context of the modeling for control design purposes as proposed in this thesis, the four assumptions for finding an analytical solution do not detract from the validity and usefulness of the proposed design methods. The analytical obtained models are valid models, with the small variations between analytical and experimental results explicable by the assumptions made.

2.4 Modal Analysis Using ANSYS (Numerical Models)

The previous section shows that modal analysis can be used to find the solution of a cantilever beam with loads attached at arbitrary positions. However, it can be seen from (2.52) that the determinant of a matrix needs to be solved to find the frequency equation of the structure. The dimension of the matrix increases with an increase in the number of the attached loads, which increases the complexity of the matrix. This complexity is associated with an increase in the number of terms in the frequency equation as shown in (2.71) and (2.73). Increasing the number of loads from one to two, causes the number of terms in the frequency equation to increase from 10 to 45. For more than two attached loads, the frequency equation becomes very long. Therefore, even though the analytical method provides a solution for finding the natural frequencies of a cantilever beam with n attached masses at arbitrary positions, it is impractical and computationally intense.

In practice, especially for complex structures, a software tool such as ANSYS can be used to find the natural frequencies of the structures. ANSYS uses the finite-element method (FEM) to solve the underlying governing equations and the associated problem-specific boundary conditions. FEM tools are used widely in industry to simulate the responses of a physical system to structural loading, and thermal and electromagnetic effects. In this research, ANSYS software version 9.0 is used to find the natural frequencies of the flexible beam with varying load conditions and the results are validated through comparison with the results from the analytical method.

The natural frequencies of the models are obtained using modal analysis in ANSYS. For comparison purposes, the first three natural frequencies of the models are shown along the results from the analytical solution in Table 2.6. From

Model	Results from ANSYS (Hz)	Results from analytical (Hz)	error(%)
1	5.9752	5.9726	0.04
	45.2360	45.2367	0.0015
	133.50	133.48	0.015
2	6.8345	6.834	0.0073
	53.8710	53.8702	0.0015
	162.86	162.87	0.0061
3	7.7432	7.7416	0.02
	59.2430	59.2439	0.0015
	145.3400	145.3532	0.009
4	10.0200	10.0176	0.02
	62.7920	62.7934	0.002
	175.8000	175.8200	0.01

Table 2.6: Comparison of natural frequency results from ANSYS with results from analytical method.

the comparison, it can be seen that the difference between the results from the analytical method and the results from ANSYS are very small (maximum 0.02%). From this comparison it can be concluded that the ANSYS results are accurate. Based on the accuracy of the results, numerical models from ANSYS will be used here to form simulation models for the experimental plant.

2.5 Simulation Models

In this research, computer simulation using Simulink is used to design and evaluate the proposed controllers. The simulation results are then used as a benchmark for real-time implementation of the proposed controllers in the experimental plant. To use Simulink as a simulation platform, the numerical models from ANSYS need to be modified into simulation models in the form of transfer functions or state space equations.

In this section simulation models to represent the experimental plant (Model 1 to Model 4) are designed and implemented. The simulation models are created in transfer functions form. A description on how to obtain the transfer functions

using modal analysis in ANSYS together with the transfer functions for all the models are given in Appendix A.

In the implementation, the order of the simulation models, which is related to how many modes need to be included in the models, must be determined. From a control design perspective, only those modes within a particular bandwidth need to be included in the model. A seemingly natural method to determine how many modes must be included in a model is to simply ignore the modes which correspond to frequencies that lie outside of the bandwidth of interest [95]. Other methods are to use a mode selection criterion based on modal information such as damping ratios and natural frequencies [52], or to use dc gain sorting [46]. In these methods, the inclusion of modes in the model is not simply based on the frequencies of the modes, but also on how dominant the modes are in forming the overall response of the system.

In this research, mode truncation is based on the dc gain sorting method as presented in [46]. The dc gain for each mode can be obtained from (2.47) by setting $s = 0$ as explained in Appendix A. All the numerical models from ANSYS show that the first three modes of vibration are the most dominant modes, and the dc gains of the modes higher than the tenth mode are very small ($< 10^{-2}$) of the dc gain of the first three modes. Moreover, the inclusion of the first 10 modes gives a bandwidth of more than 2 kHz, which is as large as one might reasonably expect for a cantilever beam system to be controlled with an active control. Therefore, the simulation models for all the plants are based on the first ten modes, and implemented in Simulink as twentieth-order systems. When compared to the experimental results where the most dominant modes are the first three modes, the simulation models with 10 modes are adequate for representing the responses of the real plant with an active an control system where most of the disturbance frequencies are less than 2 kHz[45].

The frequency responses of the models are shown in Fig. 2.8. It can be seen that in every interval between the consecutive resonance frequencies there is a frequency where the amplitude of the frequency response function (FRF) tends to zero. This is the anti-resonance frequency. This is because the transfer functions of the models have alternating poles and zeros near the imaginary axis, as shown in Fig. 2.9. This frequency response is typical of a collocated system [115].

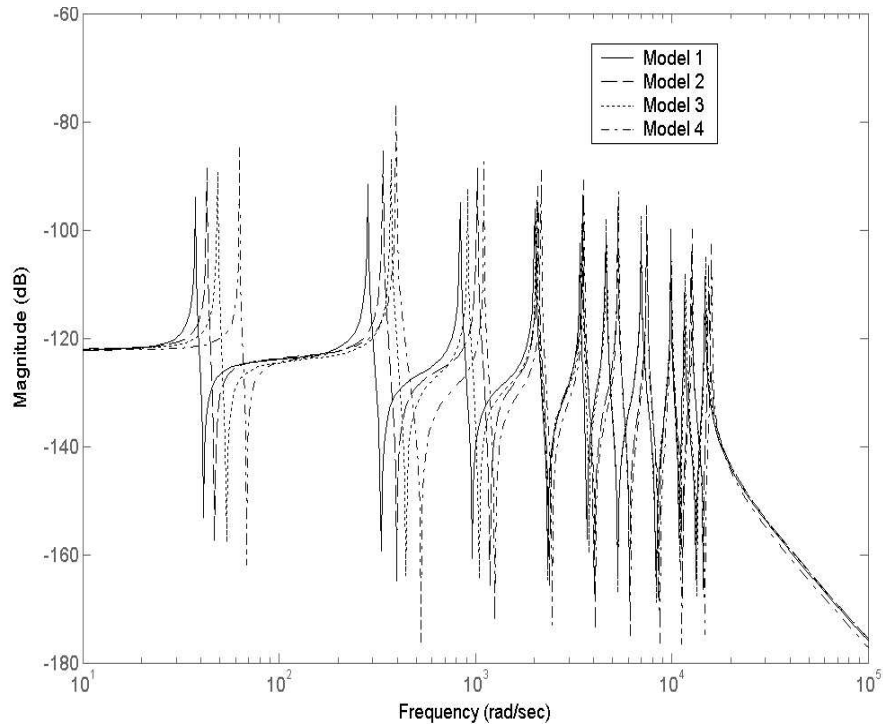


Figure 2.8. Frequency responses of simulation models.

Remark 2.1. A collocated system is obtained by the collocated placement of sensor-actuator pairs. One advantage of a collocated system is that it is always asymptotically stable for a wide class of single-input single-output (SISO) control systems even if the system parameters are subject to large perturbations [115].

The experiments with the experimental models and the results from the simulation models show that the most dominant modes are the first three modes.

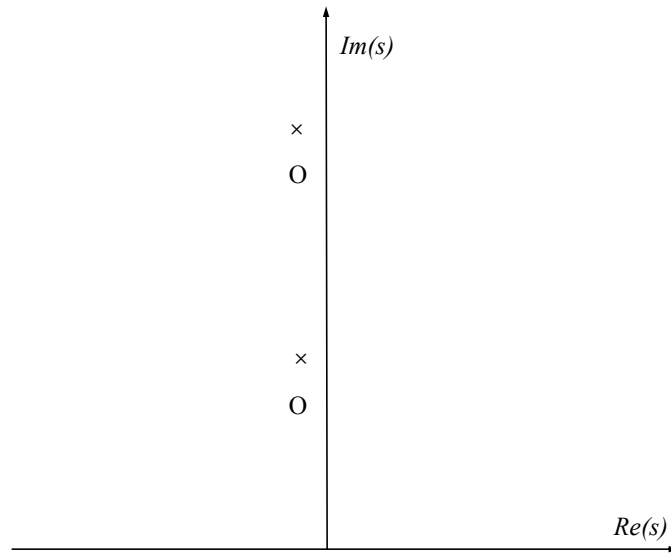


Figure 2.9: Alternating pole-zero pattern of flexible structures with collocated sensor and actuator.

Based on this, the proposed controllers will be designed to attenuate the first three modes of vibration. Therefore, it is necessary to ensure that the contributions of modes higher than the first three are negligible to the overall vibration. To show that the modes higher than the first three modes would have insignificant effect on the overall responses of the system, simulations that compare the responses of three-mode models with ten-mode models for different input signals are conducted.

Two types of signal are chosen as input signals: white noise and pulses. White noise is used as an input signal to give a uniform amplitude over a wide range of frequencies and to make sure that all the modes are excited with approximately the same amplitude. The pulse signal is used to observe the responses of the systems when subjected to impulse or shock. This type of signal contains higher harmonics, which can be expected to excite the higher modes and contribute to the overall vibration. To approximate an impulse signal, a pulse signal with short duration is used in the simulation. A pulse signal with duration 0.05 second is chosen, because for shorter durations, the models would not respond due to dead-

time. Of all the models, Model 1 and Model 4 are the extreme loading condition models. The responses of Model 2 and Model 3 are intermediate between those of Model 1 and Model 4. Therefore, only a three-mode model and a ten-mode model of Model 1 and Model 4 are chosen for the simulations.

Four simulations are conducted. In the first simulation, white noise is used as an input to the three-mode model and the ten-mode model of Model 1. In the second simulation the white noise is replaced by the pulse signal. The third and fourth simulations are similar to the first and second simulations with Model 1 replaced by Model 4.

The responses of the simulations are shown in Figs. 2.10 - 2.13. From the figures it can be seen that the differences between the three-mode models and the ten-mode models are very small. For a pulse signal input, the differences between the three-mode models and the ten-mode models only occurs in the first 0.05 second, corresponding to the duration of the pulse signal and it vanishes quickly after that period, as can be seen in Figs. 2.11 and 2.13. From the simulations, it can be verified that the first three modes of vibration are the most dominant modes and the contribution of the modes higher than the first three to the overall vibration are negligible. Hence, attenuating the first three modes of vibration would in this case adequately control the vibration of the flexible beam with varying load conditions. This would also be generally true for many structure encountered in practice.

To see how close the responses of the first three modes of the simulation models are to those of the experimental plant, comparisons in the frequency domain are made. In the experiments each model is excited with a combined sinusoidal signal containing signals with the frequencies corresponding to the first three natural frequencies of each model. The responses are then compared with the responses of the first three modes of the simulation models excited with the same signals.

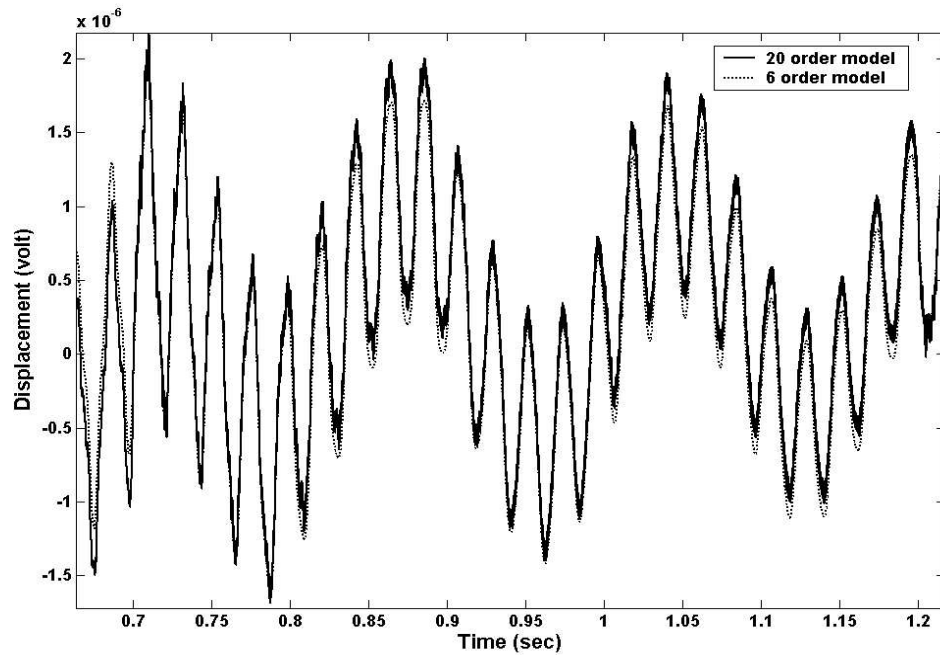


Figure 2.10: Comparative responses of the three-mode model and the ten-mode model of Model 1 with white noise input.

The comparison results are shown in Figs. 2.14 to 2.17. From the figures it can be seen that the simulation models' responses are close to the experimental plant responses. In the figures, the natural frequencies are displayed in rad/second, whereas the corresponding natural frequencies in Table 2.5 are shown in Hz. In agreement with the finding of other researchers [26, 95, 96], the simulations show that mode truncation has no effect on the natural frequency of the system. The natural frequencies of the system are still the same after the truncation. The truncation only changes the zero locations of the systems, indicated by a slightly different shape between the frequency response functions (FRFs) of experimental models and simulation models as shown in Figs. 2.14 to 2.17. Therefore, the truncated model is adequate for use as a tool for designing controllers which only need the natural frequency as a design parameter.

Figs. 2.14 to 2.17 also reveal that the vibration amplitude of the second mode

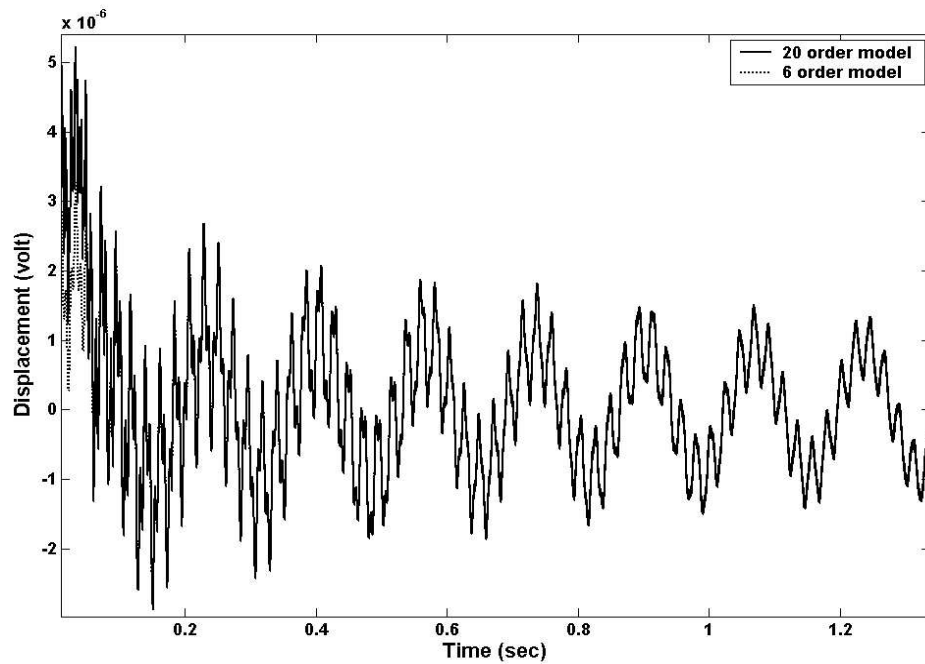


Figure 2.11: Comparative responses of the three-mode model and the ten-mode model of Model 1 with pulse signal input.

vibration for all the models is greater than those of the first and third modes. This phenomenon occurs due to the placement of the sensor-actuator pair close to the root of the cantilever beam as stated in Section 2.2. Close to the root of the beam, the curvatures for the second mode vibration for all the models are the largest, as can be seen from the mode shape of the simulation models shown in Figs. 2.18 to 2.21.

2.6 Summary

In this chapter an experimental plant and simulation models of the plant are implemented. To obtain the simulation models of the experimental plant several steps are undertaken. In the first step, the frequency equation of the system is solved analytically using the frequency determinant method, and the natural frequencies of the system are obtained graphically. In the next step, numerical

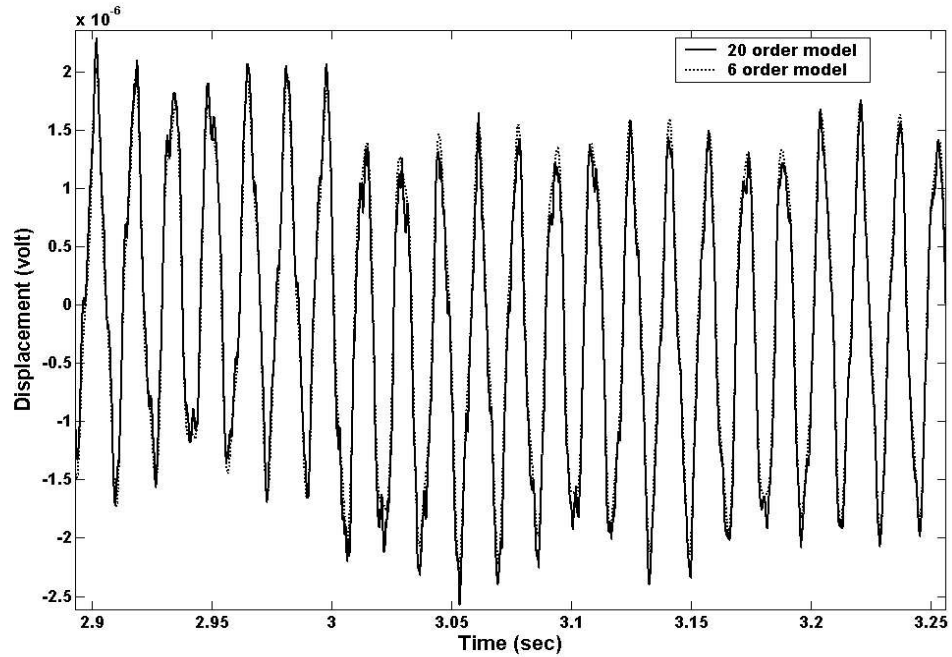


Figure 2.12: Comparative responses of the three-mode model and the ten-mode model of Model 4 with white noise input.

models obtained from modal analysis using ANSYS are compared to the analytical results to verify the validity and accuracy of the ANSYS generated models. In the last step, the simulation models are implemented in transfer function form in Simulink.

Comparisons show that the responses for the simulation models are in agreement with the responses for the experimental plant. The following conclusions can be drawn from the results:

- The first three modes of the system are the dominant modes, and the contributions of the higher modes to the overall vibration are negligible. Therefore, it would be sufficient to suppress the vibration of the first three modes to control the vibration of the flexible beam considered in this research.
- In the modeling process, the loading effects of the piezoceramic patches on

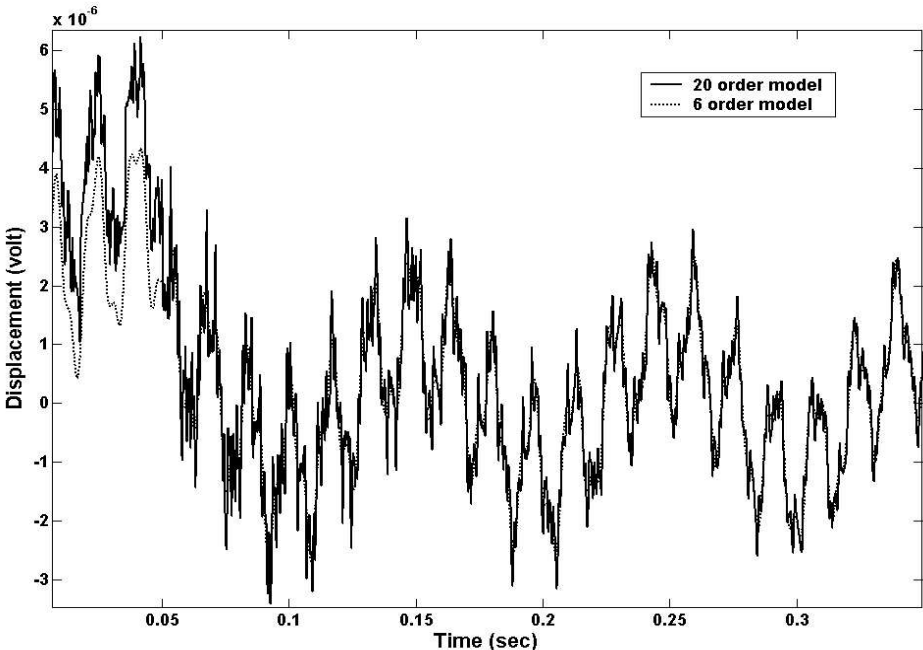


Figure 2.13: Comparative responses of the three-mode model and the ten-mode model of Model 4 with pulse signal input.

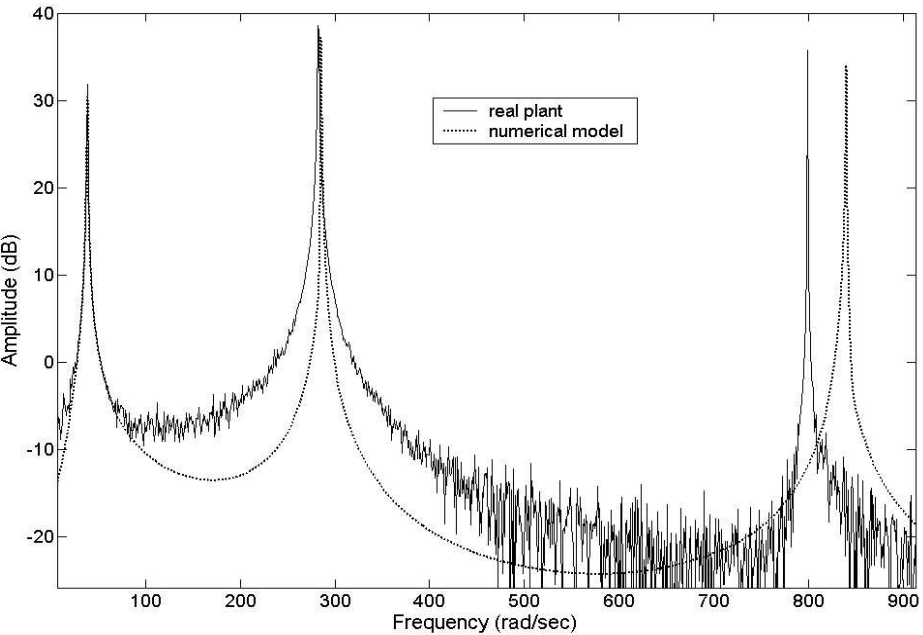


Figure 2.14: Comparative responses of real plant and simulation model for Model 1.

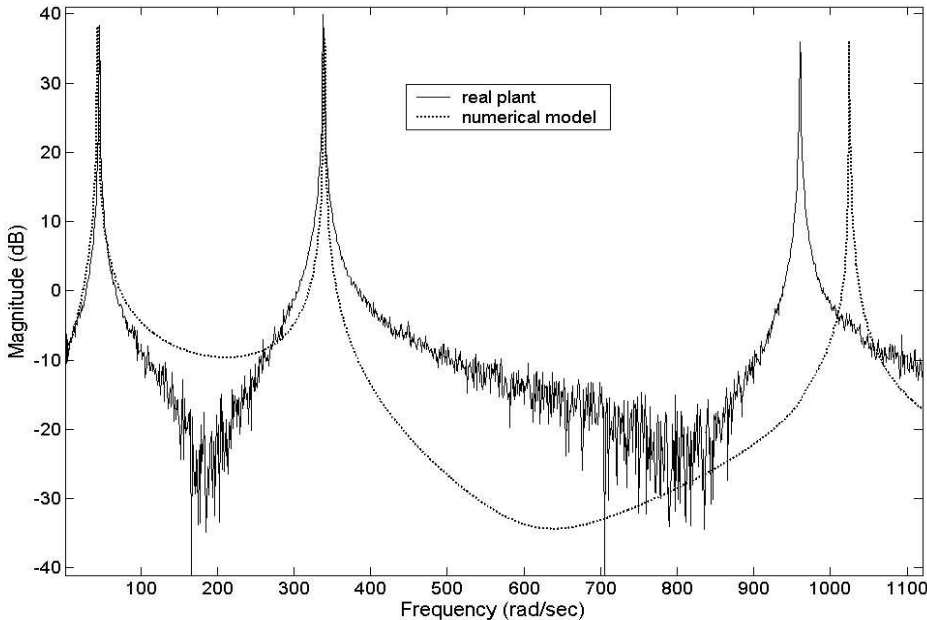


Figure 2.15: Comparative responses of real plant and simulation model for Model 2.

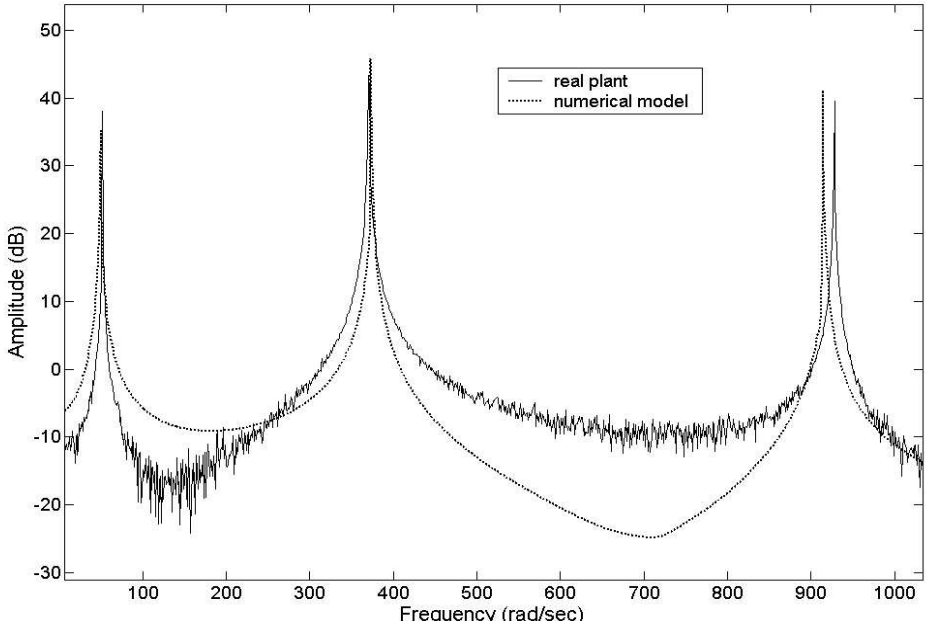


Figure 2.16: Comparative responses of real plant and simulation model for Model 3.

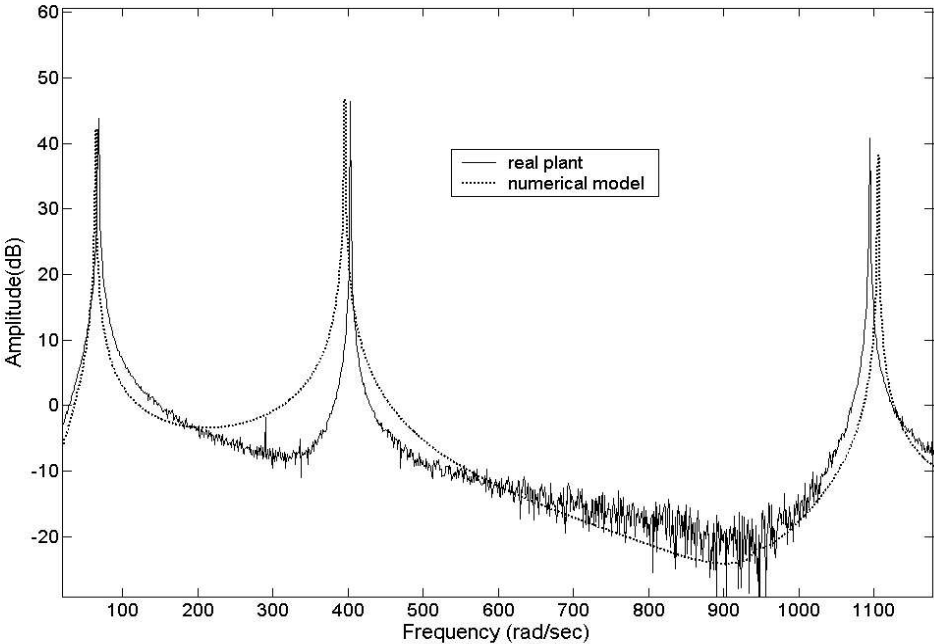


Figure 2.17: Comparative responses of real plant and simulation model for Model 4.

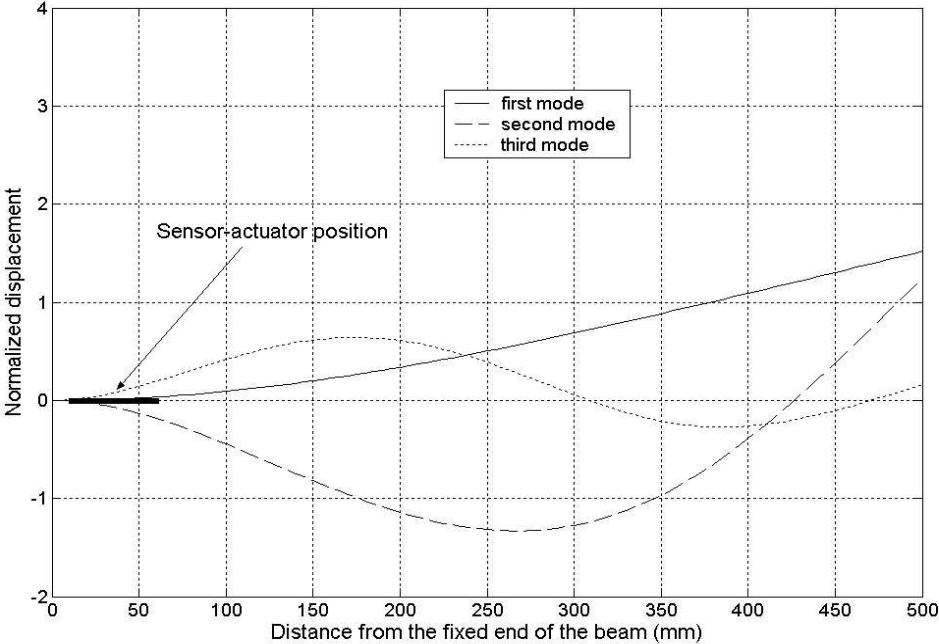


Figure 2.18. Mode shapes for Model 1.

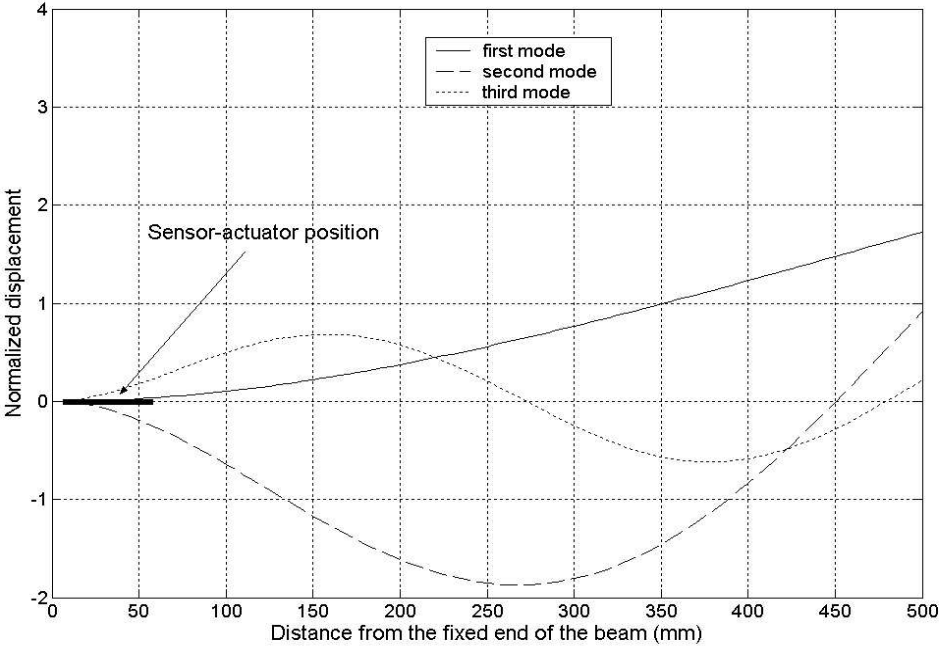


Figure 2.19. Mode shapes for Model 2.

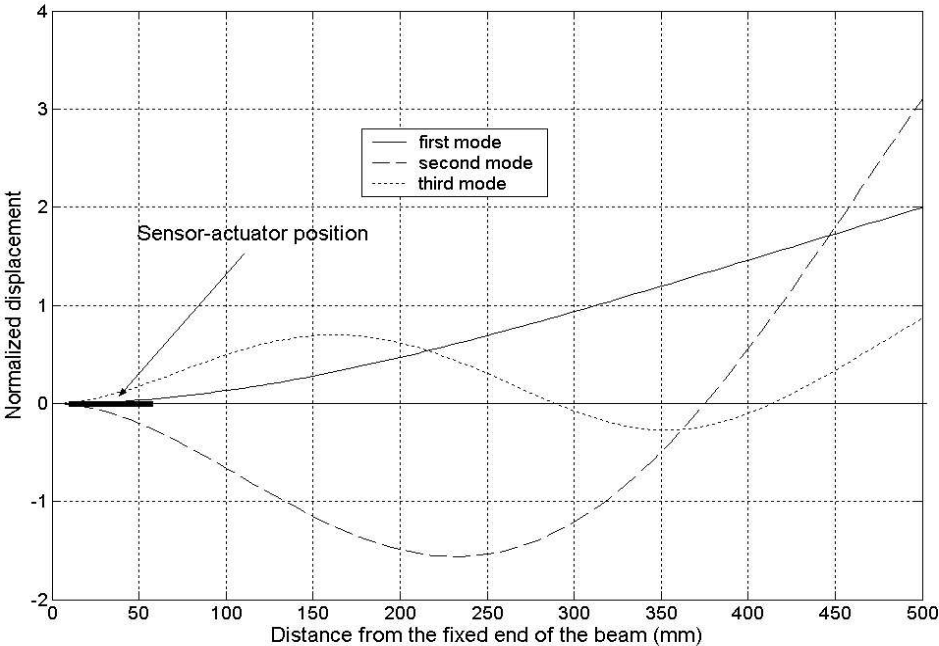


Figure 2.20. Mode shapes for Model 3.

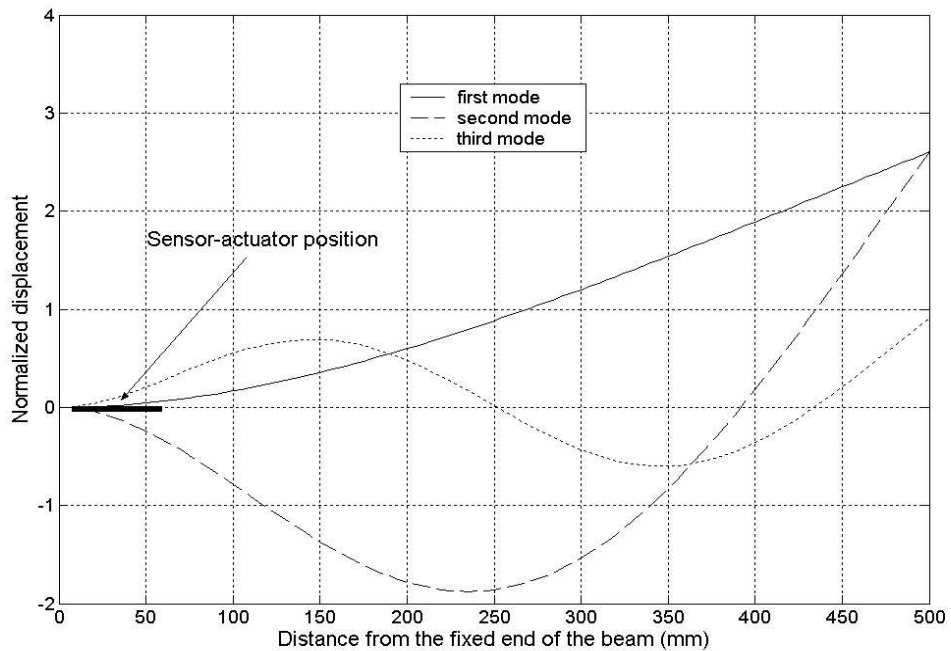


Figure 2.21. Mode shapes for Model 4.

the accuracy of the natural frequencies of the models are determined to be negligible. The objective of the modeling in this research is to obtain reasonable and usable models that can be used for control design. All the proposed controllers considered in this research only require the natural frequency as the design parameter. Therefore, neglecting the patch loading effect in the modeling is valid for the purposes of the resonant controller design.

- Mode truncation in the modeling process does not affect the accuracy of the natural frequency estimates for the structure. Therefore, for the design of controllers such as resonant controller that only use the natural frequency as the design parameter, truncated models are sufficient.